

# Fermion bag approach to Hamiltonian lattice field theories in continuous time

Emilie Huffman and Shailesh Chandrasekharan

*Duke University, Durham, North Carolina 27708, USA*

(Received 6 October 2017; published 4 December 2017)

We extend the idea of fermion bags to Hamiltonian lattice field theories in the continuous time formulation. Using a class of models we argue that the temperature is a parameter that splits the fermion dynamics into small spatial regions that can be used to identify fermion bags. Using this idea we construct a continuous time quantum Monte Carlo algorithm and compute critical exponents in the  $3d$  Ising Gross-Neveu universality class using a single flavor of massless Hamiltonian staggered fermions. We find  $\eta = 0.54(6)$  and  $\nu = 0.88(2)$  using lattices up to  $N = 2304$  sites. We argue that even sizes up to  $N = 10,000$  sites should be accessible with supercomputers available today.

DOI: [10.1103/PhysRevD.96.114502](https://doi.org/10.1103/PhysRevD.96.114502)

## I. INTRODUCTION

Quantum Monte Carlo methods of studying strongly correlated fermion systems are known to be notoriously difficult [1]. Even if sign problems can be solved it is difficult to study large system sizes close to critical points, especially when the system contains long range fermionic correlations. Many strongly interacting quantum critical points were predicted long ago in  $2 + 1$  dimensions in the presence of massless Dirac fermions [2,3], but their properties have not yet been determined accurately using quantum Monte Carlo methods. Due to developments in condensed matter physics related to the physics of graphene and the associated developments in topological insulators the field has become interesting again and there is new impetus to study the critical points better [4–7].

Studies based on the Lagrangian formulation on space-time lattices use the hybrid Monte Carlo (HMC) algorithm [8–11]. Although it is expected to have better scaling properties with system size compared to other fermion algorithms, it encounters singularities in the presence of massless fermions, especially near strongly interacting quantum critical points. In order to avoid such singularities, studies include a fermion mass. The presence of two infrared scales, in the form of a fermion mass and a finite lattice size, makes accurately extracting the critical exponents difficult. Ways to circumvent these problems would be very helpful.

Lagrangian formulations have other limitations as well. Ultralocal actions on space-time lattices can create extra doubling of fermion degrees of freedom due to time discretization. Along with chiral symmetry some internal flavor symmetries may also be lost. For example, the semimetal insulator phase transition in graphene was studied recently using the Lagrangian formulation with staggered fermions [12–14]. While these formulations capture many interesting physics qualitatively, the  $SU(2)$  spin symmetry of graphene is explicitly broken, which may affect the critical behavior. Recently, Lagrangian formulations of Dirac

fermions in  $2 + 1$  dimensions have begun to use overlap or domain wall fermions [15–17]. While these formulations preserve many symmetries of continuum Dirac fermions, they are computationally much more expensive, especially near strongly coupled quantum critical points.

We can circumvent some of the limitations of Lagrangian formulations by constructing the partition function starting from a lattice Hamiltonian. Since we can eliminate time discretization errors we can avoid an extra fermion doubling and preserve more symmetries [18–20]. Also, unlike the HMC approach the auxiliary field Monte Carlo (AFMC) methods used in the Hamiltonian formulation can also work with exactly massless fermions without encountering singularities [21,22]. In principle, the time to perform a single sweep in AFMC can be reduced to scale as  $\beta N^3$  where  $N$  is the number of spatial sites and  $\beta$  is the inverse temperature. However, there can be bottlenecks due to numerical instabilities on large lattices. Several recent studies of semimetal-insulator phase transitions in  $2 + 1$  Dirac systems have emerged recently using this approach [23–25], and the largest lattices explored are roughly of the order of  $N = 2500$  on honeycomb lattices and  $N = 1600$  on square lattices [26]. Calculations in the continuous time limit involve much smaller sizes. Although the HMC algorithm continues to be improved for Hamiltonian formulations, problems related to the singularities mentioned above have remained a bottleneck until now [27–29].

A few years ago one of us proposed a new idea called the fermion bag approach as an alternative way to construct fermion algorithms [30,31]. The idea was originally formulated within the Lagrangian formulation and has allowed us to study large lattices with exactly massless Dirac fermions and accurately extract critical exponents at some of the quantum critical points in  $2 + 1$  dimensions [32,33]. In this work we extend the idea to Hamiltonian formulations in continuous time. Using it we are able to study lattices containing up to  $N = 10,000$  sites without encountering

numerical instabilities. Although computing quantities close to quantum critical points on such large lattices still requires supercomputers, we are able to study square lattices with up to  $N = 2304$  sites on small computer clusters.

## II. IDEA OF FERMION BAGS

The idea of fermion bags is based on the intuition that it should be possible to write a fermionic partition function as a sum over weights of configurations where each configuration weight is obtained as a product of weights of smaller configurations. This is accomplished by dividing the fermion degrees of freedom of the entire system into many smaller entangled regions (or fermion bags) that are essentially independent of each other [30]. The fermion bag weight is obtained by summing over all quantum fluctuations within the bag. If this weight is positive an efficient Monte Carlo algorithm could be designed. The idea of fermion bags is an extension of the meron cluster approach [34].

While the idea of fermion bags is widely applicable there is no unique recipe to identify the bags for a given model. One guiding principle is that weights of fermion bags must be positive (which is not always guaranteed). One can also use efficiency of Monte Carlo sampling as the other guiding principle. If the fermion bags can identify the entanglement that arises naturally from the underlying physics and fermion bag weights remain positive, then the Monte Carlo sampling usually becomes efficient. For example, fermion bags can be identified differently at strong couplings as compared to weak couplings. At weak couplings Feynman diagrams suggest a natural choice for the fermion bags and then the approach is identical to the determinantal diagrammatic Monte Carlo methods [35–37]. But such an identification leads to inefficient Monte Carlo sampling at stronger couplings since the entanglement of the fermion degrees of freedom changes. Efficiency can be improved by combining weak and strong coupling fermion bags at intermediate couplings.

Recently we discovered that the idea of fermion bags can be useful even if a fermion bag becomes entangled with the rest of the system. We realized that this entanglement can be stored in the form of a large matrix. If this can be computed and stored we can perform fast updates of fermion bags. This extension of the fermion bag idea is similar to the idea of local factorization of the determinant proposed recently [38]. In our case it has allowed us to study  $60^3$  lattices near a quantum critical point with exactly massless fermions for the first time [39]. In this work we argue that a similar idea should be applicable for Hamiltonian lattice fermions.

In order to illustrate how the idea of fermion bags can be extended to Hamiltonian formulations in continuous time, in this work we focus on those that can be written as  $H = \sum_{x,d} H_{x,d}$  where

$$H_{x,d} = -\omega_{\langle x,d \rangle} e^{2\alpha_{\langle x,d \rangle}} \sum_{a=1}^{N_f} (c_x^{a\dagger} c_{x+\hat{d}}^a + c_{x+\hat{d}}^a c_x^a). \quad (1)$$

Here  $x$  is a spatial lattice site;  $\hat{d}$  labels the directions such that  $\langle x, d \rangle$  labels a unique nearest neighbor bond. The operators  $c_x^{a\dagger}$  and  $c_x^a$  are fermionic creation and annihilation operators at the site  $x$  with a flavor  $a = 1, 2, \dots, N_f$ . The couplings of the model are defined through the real constants  $\omega_{\langle x,d \rangle} > 0$  and  $\alpha_{\langle x,d \rangle}$ . In the discussions below we focus on the  $N_f = 1$  model on a two-dimensional square lattice with periodic boundary conditions and  $L$  sites in each direction with  $N = L^2$ . However, they can be extended to any value of  $N_f$  and all bipartite lattice models where the sites connected to the bond  $\langle x, d \rangle$  lie on different sublattices.

Although the Hamiltonians we consider are unconventional they contain rich physics. We have designed them so that the idea of fermion bags is applicable [40]. For a fixed  $N_f$  they are invariant under an  $O(2N_f)$  flavor symmetry in addition to the usual lattice symmetries, some of which may be broken spontaneously at quantum critical points [41]. When  $N_f = 1$  our model is equivalent (up to a constant) to the model (sometimes referred to as the  $t - V$  model in the literature),

$$H_{x,d} = -t\eta_{x,d}(c_x^\dagger c_{x+\hat{d}} + c_{x+\hat{d}}^\dagger c_x) - V\Phi_x\Phi_{x+\hat{d}}, \quad (2)$$

where  $V > 0$ . Here we define  $\Phi_x = (-1)^{x_1+x_2}(c_x^\dagger c_x - 1/2)$ , assuming a lattice site with coordinates  $x = (x_1, x_2)$ . The equivalence requires that we set  $\omega_{\langle x,d \rangle} = t^2/(V(1 - (V/2t)^2))$ , and  $\alpha_{\langle x,d \rangle} = \alpha\eta_{x,d}$  where  $\cosh 2\alpha = (1 + (V/2t)^2)/(1 - (V/2t)^2)$ , and  $\sinh 2\alpha = (V/t)/(1 - (V/2t)^2)$  [42]. If we define  $\eta_{\langle x,1 \rangle} = 1$  and  $\eta_{\langle x,2 \rangle} = (-1)^{x_1}$ , the model describes interacting two-dimensional massless Hamiltonian staggered fermions [43].

Using the well-known CT-INT expansion of the partition function [18–20] we can write

$$Z = \sum_k \int [d\tau] \sum_{\{[x,d]\}} \text{Tr}(H_{x_k,d_k} \dots H_{x_2,d_2} H_{x_1,d_1}), \quad (3)$$

where there are  $k$  insertions of the bond Hamiltonian  $H_{x,d}$  inside the trace at times  $\tau_1 \leq \tau_2 \leq \dots \leq \tau_k$ . The symbol  $[d\tau]$  represents the  $k$  time-ordered integrals and  $\{[x,d]\} = \{\langle x_1, d_1 \rangle, \langle x_2, d_2 \rangle, \dots, \langle x_k, d_k \rangle\}$  represents the configuration of bonds at different times. Since a configuration of bonds also requires the information of the times where the bonds are inserted we label the configuration as  $[x, d, \tau]$ . An illustration of a bond configuration is shown in Fig. 1. Each bond represents the operator  $H_{x,d}$  that is present inside the trace in (3). It can be shown that the traces that appear in (3) are always positive [44,45].

We can imagine  $H_{x,d}$  as creating a quantum entanglement between the fermions at  $x$  and  $x + \hat{d}$ . Thus, all spatial

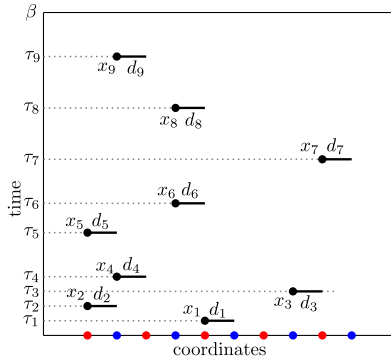


FIG. 1. An example configuration. The horizontal axis labels the spatial sites; the vertical axis is imaginary time.

sites connected by bonds to each other at various times become entangled with each other. Such a group of entangled sites can be defined as a fermion bag. For the bond configuration in Fig. 1 we identify four fermion bags as shown in Fig. 2. When two bonds  $x, d$  and  $x', d'$  do not share a site between them the bond Hamiltonians commute, i.e.,  $[H_{x,d}, H_{x',d'}] = 0$ . This implies that the weight of the bond configuration can be written as a product of weights from fermion bags.

Since the space-time density of bonds is a physical quantity related to the energy density of the system [42], for every coupling  $V$  we expect a fixed density of bonds. This implies that we can use the temperature as a parameter to control the size of fermion bags. At high temperatures we have fewer bonds and many small fermion bags. Note that lattice sites that are not connected to any bonds form their own fermion bags. As the temperature is lowered fermion bags will begin to merge to form a single large fermion bag. At very low temperatures there will only be a few isolated small fermion bags. This suggests that at some optimal temperature the fermion bags may efficiently break up the system into smaller regions that do not depend on the system size. Even at low temperatures, we may be able to divide the imaginary time axis into many time slices and update a single time slice efficiently. This is illustrated in Fig. 3,

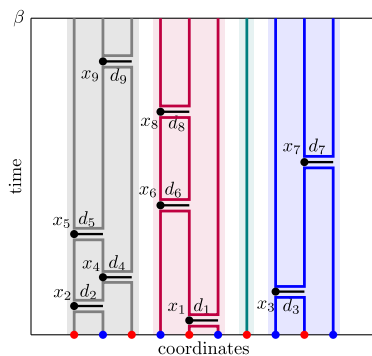


FIG. 2. The bonds in this configuration form four fermion bags between  $\tau = 0$  and  $\tau = \beta$ .

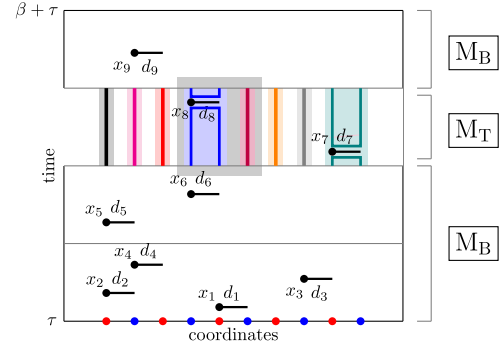


FIG. 3. Time slices are added and  $M_T$  and  $M_B$  regions defined. Fermion bags are highlighted in the  $M_T$  region, and the current update block is shaded.

where the imaginary time extent is divided into four time slices and in the shaded time slice there are eight fermion bags, instead of the four shown in Fig. 2. While there seems to be a connection of the fermion bag size to a notion of a percolation transition, as far as we know nothing physical occurs at this transition.

In order to test if the maximum fermion bag size remains independent of the lattice size even for large lattices we have studied the  $t - V$  model (2) on a square lattice near its critical point. Taking  $\beta = 4.0$  we divided the imaginary time direction into 16 time slices and studied the fermion bag size as a function of the lattice size. For equilibrated configurations of  $L = 48, 64$  and  $100$ , the average maximum fermion bag size within a time slice was about 30, independent of  $L$ . Further tests suggest that the optimal temperature is roughly 0.25. Since bond insertions in different fermion bags commute with each other, we can efficiently update fermion bags in space-time blocks (shown as a box in the shaded time slice in Fig. 3) involving 30 to 60 spatial sites within each time slice. During this update the effects of the bonds outside this block are taken into account through the fixed  $N \times N$  matrix as we discuss in the next section.

### III. ALGORITHM AND UPDATES

We now discuss our Monte Carlo algorithm to calculate the correlation observable

$$\langle C \rangle = \text{Tr}(\Phi_{(0,0)} \Phi_{(L/2,0)} e^{-\beta H}) / \text{Tr}(e^{-\beta H}) \quad (4)$$

to illustrate the advantages of the fermion bag approach. This observable is used in the next section to study the quantum critical behavior of the  $t - V$  model. In our algorithm we generate configurations  $([x, d, \tau]; \tau_0)$  in two sectors: the partition function sector ( $n = 0$ ) with weight  $\Omega_0([x, d, \tau]; \tau_0)$  and the observable sector ( $n = 1$ ) with weight  $f\Omega_1([x, d, \tau]; \tau_0)$  where

$$\Omega_n([x, d, \tau]; \tau_0) = \text{Tr}[H_{x_k, d_k} \dots C_n \dots H_{x_2, d_2} H_{x_1, d_1}]. \quad (5)$$

Here  $0 \leq \tau_0 \leq \beta$  is a time where the operator  $C_n$  is introduced. In the partition function sector  $C_0 = I$  (the identity operator) and in the observable sector  $C_1 = \Phi_{(0,0)} \Phi_{(L/2,0)}$ . The factor  $f > 0$  is chosen so that the two sectors can be sampled with roughly equal probabilities. We record the number

$$\mathcal{N} = \frac{\Omega_1([x, d, \tau]; \tau_0)}{\Omega_0([x, d, \tau]; \tau_0) + f\Omega_1([x, d, \tau]; \tau_0)} \quad (6)$$

for each configuration generated. It is easy to prove that  $\langle C \rangle = \langle \mathcal{N} \rangle / (1 - f\langle \mathcal{N} \rangle)$ .

We use four different types of updates to generate the configurations  $([x, d, \tau]; \tau_0)$  in the two sectors, which are detailed in [46]. Each sweep consists of at least one of each of these four updates. The two most time intensive updates are the sector update and the bond update: the sector update flips the sector  $n \rightarrow 1 - n$  while keeping  $([x, d, \tau]; \tau_0)$  fixed, and the bond update changes the entire bond configuration  $[x, d, \tau] \leftrightarrow [x', d', \tau']$  while keeping  $t_0$  and  $n$  fixed. For these updates we need to compute the ratio  $R = \Omega_n([x, b, \tau]; \tau_0) / \Omega'_n([x', b', \tau']; \tau_0)$  to calculate the transition probabilities in the Metropolis accept/reject step. Since the sector update is a special case of the bond update we only focus on the details of the bond updates. Using the Blankenbecler-Scalapino-Sugar (BSS) formula [47] we can show

$$\Omega_n([x, d, \tau]; \tau_0) = \det(\mathbb{1}_N + B_{x_k, d_k} \dots O_n \dots B_{x_2, d_2} B_{x_1, d_1}), \quad (7)$$

where  $\mathbb{1}_N$ ,  $B_{x_i, d_i}$  and  $O_n$  are all  $N \times N$  matrices with rows and columns labeled by spatial lattice sites. The matrix  $\mathbb{1}_N$  is the identity matrix, while  $B_{x_i, d_i}$  is the identity matrix except in a  $2 \times 2$  block labeled by the rows and columns of the sites that touch the bond  $\langle x_i, d_i \rangle$ . Within this block,  $B_{x_i, d_i}$  takes the form

$$B_{x,d} = \begin{pmatrix} \cosh 2\alpha & \eta_{x,d} \sinh 2\alpha \\ \eta_{x,d} \sinh 2\alpha & \cosh 2\alpha \end{pmatrix}. \quad (8)$$

Finally, the matrix  $O_n$  depends on the sector  $n$  and is given by  $O_0 = \mathbb{1}_N$  and  $(O_1)_{x,y} = \delta_{x,y} - 2\delta_{x,(0,0)} - 2\delta_{x,(L/2,0)}$ .

Before we begin the bond update we divide the configuration space into time slices of width 0.25 with  $t_0$  chosen to be at the beginning of the first time slice. We then update bonds within each time slice sequentially. During the update of a time slice we define two  $N \times N$  matrices: the background matrix  $M_B$  (which is a product of all of the  $B_{x,d}$  matrices outside the selected time slice and  $O_n$ ), and the time-slice matrix  $M_T$ , which is the product of all the  $B_{x,d}$  matrices within the time slice being updated. Figure 3 shows what contributes to  $M_B$  and  $M_T$ . When the configuration of bonds within the time slice is changed then only  $M_T$  changes to  $M'_T$ . The ratio  $R$  is given by

$$R = \frac{\det(\mathbb{1}_N + M_B M'_T)}{\det(\mathbb{1}_N + M_B M_T)} = \det(\mathbb{1}_N + G_B \Delta), \quad (9)$$

where we have defined two new  $N \times N$  matrices  $G_B = (\mathbb{1}_N + M_B M_T)^{-1} M_B M'_T$  and  $\Delta = (M_T^{-1} M'_T - \mathbb{1}_N)$ . Since the bond matrices  $B_{x,d}$  in different fermion bags commute, it is easy to verify that  $\Delta$  is nonzero only within a block which contains spatial sites connected to fermion bags that change. If we randomly choose a spatial block containing about 30–60 sites and focus on updating the bonds only within that block, during such a block update the size of the matrix  $\Delta$  cannot be greater than the sum of the sites in the fermion bags that touch the sites within the block. We refer to this set of sites, which can be larger than the block size, as a superbag and denote its size as  $s$ . Since  $\Delta$  is nonzero only in an  $s \times s$  block, it is easy to show that the computation of  $R$  (the ratio of the weight of the current configuration with that of the background configuration that existed at the time when the block update began) using (9) reduces to the computation of the determinant of an  $s \times s$  matrix. Since  $G_B$  and  $M_T$  are fixed matrices during the entire block update, they can be computed and stored. All proposals to update the current configuration within the block reduce to taking the determinant of an  $s \times s$  matrix, independent of system size. Details for how to update  $G_B$  in a stable way can be found in [46].

The time to complete a single sweep with our algorithm scales as  $\beta N^3$ , which is similar to the traditional auxiliary field algorithms. However, using the idea of fermion bags we have reduced the prefactor significantly as explained in [46]. In Fig. 4 we show equilibration of  $N_b$  (the total

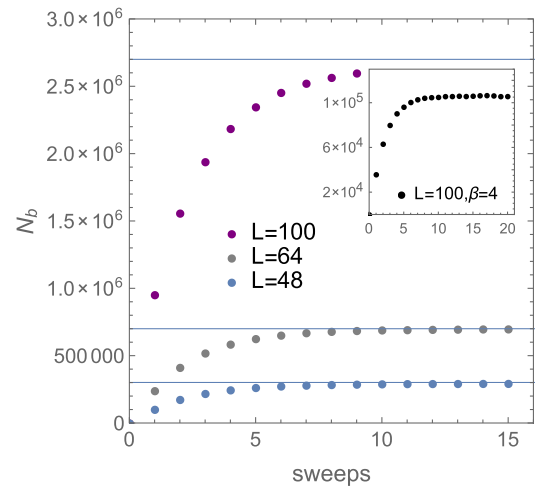


FIG. 4. Plot showing  $\beta = L$  equilibration of the total number of bonds  $N_b$  in a bond configuration starting from 0, as a function of Monte Carlo sweeps. The horizontal lines show the expected equilibrated values. The time for a single bond update on a single core is approximately 30 days for  $L = 100$ , 30 hours for  $L = 64$ , and 4 hours for  $L = 48$ . The inset shows equilibration at  $L = 100$ ,  $\beta = 4$ .

number of bonds in a configuration) as a function of sweeps for  $\beta = L = 48, 64, 100$  and  $V = 1.304t$ . Although the  $L = 100$  data have not equilibrated, there is no bottleneck (see the inset of Fig. 4). We estimate the bond density at equilibrium to be  $N_b/\beta L^2 \approx 2.7$ , which means at  $L = \beta = 100$  we will have roughly 2.7 million bonds after equilibration. A single sweep thus roughly requires a month on a single 3 GHz CPU core.

#### IV. RESULTS AT CRITICALITY

Using the algorithm described above, we have studied the two-dimensional  $t - V$  model and computed the critical exponents at the quantum phase transition between the massless and the massive fermion phases. These critical exponents are expected to belong to the Ising Gross-Neveu universality class with  $N_f = 1$  four-component Dirac fermions [48–50]. For large values of  $L$  we expect the observable  $\langle C \rangle$  to scale as  $L^{-4}$  in the massless phase and to saturate to a constant in the massive phase. In the critical region ( $V \approx V_c$  and large values of  $L$ ) we expect  $\langle C \rangle$  to satisfy the leading critical finite size scaling relation [51,52]

$$\langle C \rangle = \frac{1}{L^{1+\eta}} f((V - V_c)L^{1/\nu}/t). \quad (10)$$

Our Monte Carlo results are consistent with the expectations.

Table I shows our results for  $\langle C \rangle$  as a function of  $V$  and  $L$  near the critical point where we set  $\beta = L$ . Approximating  $f(x) = f_0 + f_1x + f_2x^2 + f_3x^3$ , we perform a seven parameter combined fit of the data given in Table I, except the  $L = 32$  data at  $V = 1.4$ , which does not seem to lie within the scaling window. From the fit we obtain  $\eta = 0.54(6)$ ,  $\nu = 0.88(2)$ ,  $V_c = 1.279(3)t$ ,  $f_0 = 0.77(11)$ ,  $f_1 = 0.30(4)$ ,  $f_2 = 0.052(8)$ , and  $f_4 = 0.0033(6)$ . The  $\chi^2/\text{DOF}$  for the fit is 0.8. We show the data and the scaling fit in the left plot of Fig. 5. Theoretical exponent predictions are compatible with our results [48,49].

The  $t - V$  model we study here has been studied earlier on smaller lattices by two groups. Not surprisingly, the

TABLE I. Our Monte Carlo results for the  $t - V$  model (2) on a square lattice with  $20 \leq L \leq 48$  and  $\beta = L$ .

$V/t$	$L = 20$	$L = 24$	$L = 32$	$L = 48$
1.200	0.00298(3)	0.00184(3)	0.00080(1)	...
1.250	0.00545(6)	0.00380(5)	0.00204(2)	0.00074(2)
1.270	0.00699(8)	0.00517(7)	0.00315(4)	0.00151(3)
1.296	0.00946(10)	0.00740(9)	0.00512(6)	0.00339(5)
1.304	0.01022(8)	0.00844(9)	0.00611(6)	0.00423(5)
1.350	0.01705(16)	0.01522(16)	0.01426(18)	...
1.400	0.02707(20)	0.02630(35)	0.02637(38)	...

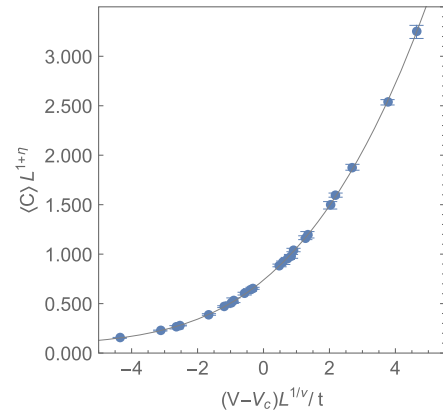


FIG. 5. Critical scaling plot showing our Monte Carlo data scaled with  $\eta = 0.54$ ,  $\nu = 0.88$ ,  $V_c = 1.279t$ . The solid line shows  $f(x) = 0.77 + 0.30x + 0.052x^2 + 0.0033x^3$ .

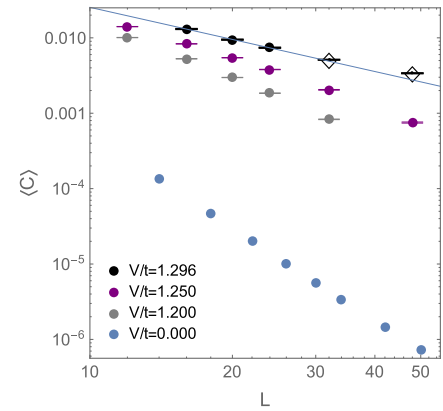


FIG. 6. Plot of  $\langle C \rangle$  as a function of  $L$  (with  $\beta = L$ ) at various values of  $V$ .  $\langle C \rangle$  scales as  $L^{-4}$  at  $V = 0$  as expected. The solid line shows the best fit for  $\langle C \rangle \sim L^{-(1+\eta)}$ .

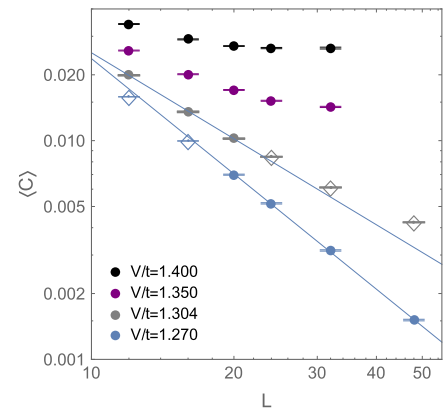


FIG. 7. Plot of  $\langle C \rangle$  as a function of  $L$  (with  $\beta = L$ ) at various values of  $V$ .  $\langle C \rangle$  saturates to a constant at  $V = 1.4t$ . The solid line shows the best fit for  $\langle C \rangle \sim L^{-(1+\eta)}$ .

critical point and the critical exponents measured are in disagreement with each other. The first calculation was performed on lattices up to  $N = 400$  sites and it was found that  $V_c = 1.304(2)$ ,  $\eta = 0.318(8)$ , and  $\nu = 0.80(6)$  [23]. In a later calculation lattices up to  $N = 484$  sites were used and it was found that  $V_c = 1.296(1)$ ,  $\eta = 0.43(2)$ , and  $\nu = 0.79(4)$  [24].

Our results are obtained from lattice sizes that are five times larger than earlier studies and suggest a lower critical point and so a higher value for the exponent  $\eta$ . The value of  $\nu$  also seems slightly higher but not inconsistent with previous results. If we exclude the larger lattice results we do find consistency with previous results. For example, if we assume  $V_c/t = 1.296$  or  $1.304$  and fit our data to the form  $L^{-(1+\eta)}$ , after dropping larger values of  $L$  we get  $\eta = 0.41(4)$  and  $\eta = 0.31(4)$  respectively with a reasonable  $\chi^2/\text{DOF}$  (see Figs. 6 and 7). However, the fits fail dramatically if  $L = 32$  and  $L = 48$ . On the other hand at  $V = 1.27t$  the data fit well for larger values of  $L$  and give us  $\eta = 0.74(2)$ . If we force  $V_c = 1.27t$  in the combined fit, the  $\chi^2/\text{DOF}$  increases to 1.3.

## V. CONCLUSIONS

In this work we have demonstrated that the idea of fermion bags can be combined with standard Monte Carlo techniques to study large system sizes in continuous time. We studied the quantum critical behavior in the simplest Ising Gross-Neveu universality class and extracted the critical exponents using lattice sizes that were five times larger than previous work. Even larger sizes are feasible with supercomputers available today. With additional research, the idea of fermion bags should be applicable to a wide class of models.

## ACKNOWLEDGMENTS

We thank F. Assaad, K. Damle, T. Grover, L. Wang, S. Wessel and U.-J. Wiese for stimulating discussions. The work is supported by the U.S. Department of Energy, Office of Science, Nuclear Physics program under Award No. DE-FG02-05ER41368. Calculations on large lattices were made possible by the Open Science Grid, supported by the National Science Foundation. E. H. is also supported by a National Physical Science Consortium fellowship.

- 
- [1] M. Troyer and U.-J. Wiese, *Phys. Rev. Lett.* **94**, 170201 (2005).
  - [2] B. Rosenstein, B. J. Warr, and S. H. Park, *Phys. Rev. Lett.* **62**, 1433 (1989).
  - [3] B. Rosenstein, B. J. Warr, and S. H. Park, *Phys. Rep.* **205**, 59 (1991).
  - [4] I. F. Herbut, *Phys. Rev. Lett.* **97**, 146401 (2006).
  - [5] L. Janssen and H. Gies, *Phys. Rev. D* **86**, 105007 (2012).
  - [6] B. H. Wellegehausen, D. Schmidt, and A. Wipf, *arXiv:1708.01160*.
  - [7] Y.-Z. You, Y.-C. He, C. Xu, and A. Vishwanath, *arXiv:1705.09313*.
  - [8] S. Hands, A. Kocic, and J. Kogut, *Ann. Phys. (N.Y.)* **224**, 29 (1993).
  - [9] L. Krkkinen, R. Lacaze, P. Lacock, and B. Petersson, *Nucl. Phys.* **B415**, 781 (1994).
  - [10] E. Focht, J. Jersák, and J. Paul, *Phys. Rev. D* **53**, 4616 (1996).
  - [11] S. Christofi and C. Strouthos, *J. High Energy Phys.* **07** (2007) 088.
  - [12] J. E. Drut and T. A. Lähde, *Phys. Rev. B* **79**, 165425 (2009).
  - [13] C. DeTar, C. Winterowd, and S. Zafeiropoulos, *Phys. Rev. B* **95**, 165442 (2017).
  - [14] C. DeTar, C. Winterowd, and S. Zafeiropoulos, *Phys. Rev. Lett.* **117**, 266802 (2016).
  - [15] N. Karthik and R. Narayanan, *Phys. Rev. D* **94**, 065026 (2016).
  - [16] S. Hands, *J. High Energy Phys.* **11** (2016) 015.
  - [17] S. Hands, in *Proceedings of the 35th International Symposium on Lattice Field Theory (Lattice 2017) Granada, Spain, 2017* (2017), *arXiv:1708.07686*.
  - [18] A. N. Rubtsov, V. V. Savkin, and A. I. Lichtenstein, *Phys. Rev. B* **72**, 035122 (2005).
  - [19] E. Gull, A. J. Millis, A. I. Lichtenstein, A. N. Rubtsov, M. Troyer, and P. Werner, *Rev. Mod. Phys.* **83**, 349 (2011).
  - [20] L. Wang, M. Iazzi, P. Corboz, and M. Troyer, *Phys. Rev. B* **91**, 235151 (2015).
  - [21] R. Blankenbecler, D. J. Scalapino, and R. L. Sugar, *Phys. Rev. D* **24**, 2278 (1981).
  - [22] M. Bercx, F. Goth, J. S. Hofmann, and F. F. Assaad, *SciPost Phys.* **3**, 013 (2017).
  - [23] L. Wang, P. Corboz, and M. Troyer, *New J. Phys.* **16**, 103008 (2014).
  - [24] Z.-X. Li, Y.-F. Jiang, and H. Yao, *New J. Phys.* **17**, 085003 (2015).
  - [25] S. Hesselmann and S. Wessel, *Phys. Rev. B* **93**, 155157 (2016).
  - [26] Y. Otsuka, S. Yunoki, and S. Sorella, *Phys. Rev. X* **6**, 011029 (2016).
  - [27] M. V. Ulybyshev, P. V. Buividovich, M. I. Katsnelson, and M. I. Polikarpov, *Phys. Rev. Lett.* **111**, 056801 (2013).
  - [28] M. Krner, D. Smith, P. Buividovich, M. Ulybyshev, and L. von Smekal, *arXiv:1704.03757*.
  - [29] S. Beyl, F. Goth, and F. F. Assaad, *arXiv:1708.03661*.
  - [30] S. Chandrasekharan, *Phys. Rev. D* **82**, 025007 (2010).
  - [31] S. Chandrasekharan, *Eur. Phys. J. A* **49**, 90 (2013).

- [32] S. Chandrasekharan and A. Li, *Phys. Rev. Lett.* **108**, 140404 (2012).
- [33] S. Chandrasekharan and A. Li, *Phys. Rev. D* **88**, 021701 (2013).
- [34] S. Chandrasekharan and U.-J. Wiese, *Phys. Rev. Lett.* **83**, 3116 (1999).
- [35] M. Boninsegni, N. V. Prokof'ev, and B. V. Svistunov, *Phys. Rev. E* **74**, 036701 (2006).
- [36] E. Burovski, E. Kozik, N. Prokof'ev, B. Svistunov, and M. Troyer, *Phys. Rev. Lett.* **101**, 090402 (2008).
- [37] F. F. Assaad and T. C. Lang, *Phys. Rev. B* **76**, 035116 (2007).
- [38] M. Cè, L. Giusti, and S. Schaefer, *Phys. Rev. D* **95**, 034503 (2017).
- [39] V. Ayyar and S. Chandrasekharan, *Phys. Rev. D* **93**, 081701 (2016).
- [40] R. K. Kaul, R. G. Melko, and A. W. Sandvik, *Annu. Rev. Condens. Matter Phys.* **4**, 179 (2013).
- [41] F. F. Assaad and T. Grover, *Phys. Rev. X* **6**, 041049 (2016).
- [42] L. Wang, Y.-H. Liu, and M. Troyer, *Phys. Rev. B* **93**, 155117 (2016).
- [43] L. Susskind, *Phys. Rev. D* **16**, 3031 (1977).
- [44] E. F. Huffman and S. Chandrasekharan, *Phys. Rev. B* **89**, 111101 (2014).
- [45] Z.-X. Li, Y.-F. Jiang, and H. Yao, *Phys. Rev. B* **91**, 241117 (2015).
- [46] See Supplemental Material <http://link.aps.org/supplemental/10.1103/PhysRevD.96.114502> for algorithmic details, performance, comparisons, and tests.
- [47] V. Agranovich and A. A. Maradudin, *Electronic Phase Transitions* (Elsevier Science Publishers B. V., New York, 1992), Chap. 4, pp. 177–235.
- [48] L. Rosa, P. Vitale, and C. Wetterich, *Phys. Rev. Lett.* **86**, 958 (2001).
- [49] L. N. Mihaila, N. Zerf, B. Ihrig, I. F. Herbut, and M. M. Scherer, *Phys. Rev. B* **96**, 165133 (2017).
- [50] N. Zerf, L. N. Mihaila, P. Marquard, I. F. Herbut, and M. M. Scherer, [arXiv:1709.05057](https://arxiv.org/abs/1709.05057).
- [51] *Finite Size Scaling*, edited by J. L. Cardy (1988).
- [52] M. Campostrini, A. Pelissetto, and E. Vicari, *Phys. Rev. B* **89**, 094516 (2014).